Part II Applied Physics

Section 1 Atomic, Molecular, and Optical Physics

Chapter 1. Quantum Optics and Photonics

Academic and Research Staff

Professor Shaoul Ezekiel, Dr. Selim M. Shahriar, Dr. Byoung S. Ham, Dr. Xiao-Wei Xia, Dr. Stephen P. Smith, Dr. Venkatapuram S. Sudarshanam

Visiting Scientists and Research Affiliates

Dr. M. Cronin-Golomb, Dr. Timothy T. Grove, Dr. Philip R. Hemmer, Dr. Christopher K.Y. Leung, Dr. Mara G. Prentiss, Michelle Henrion, John D. Kierstead

Graduate Students

Michael Bock, Jeffrey A. Bowers, John Donoghue, Niell G. Elvin, Yuli Friedman, Darren Hsiung, Jacob A. Morzinski, Ying Tan, Lily Wong

Undergraduate Students

Alex Bernstein, Beng-Teck Lim

1.1 Polarization Selective Motional Holeburning for High-Efficiency, Degenerate Optical Phase Conjugation in Rubidium

Sponsors

U.S. Air Force - Office of Scientific Research/
AASERT
Grant F49620-96-1-0308
U.S. Air Force - Research Laboratory
Grant F30602-97-C-0136

Optical phase conjugation (OPC) is of interest for many applications such as optical resonators, high-speed turbulence correction, and the production of the squeezed vacuum state. In the interest of practical implementation of OPC, a great deal of work has been done in the search for materials that have a fast response time, high gain, and a low power requirement. One promising candidate is an atomic vapor, because of the high degree of nonlinearity near resonance. Early efforts at performing OPC in a vapor were designed to treat the atoms as two-level systems. In order to avoid absorption losses, it was necessary to operate off-resonance, thus requiring a very high intensity.[1]

To circumvent this problem, we previously demonstrated the use of coherent population trapping[2] (CPT) as a mechanism for creating a large nonlinearity using low power. This technique allows one to obtain a suitable combination of pump power and speed. For example, we demonstrated in sodium vapor[3] a conjugate at the pump intensity of 1 W/cm^2 with reflectivity greater than 50 and a response time of less than 1 μs. As an application, we have also used this conjugator to compensate for aberrations caused by high-speed turbulence.[4] While this conjugator performed well, it required a large detuning between the pump and the probe beams, representing a serious impediment to extending this technique to other resonant media.

To eliminate this constraint, we reproduced the CPT-based conjugator using Zeeman sublevels of a single hyperfine ground state and polarized light.[5] This experiment used rubidium and matched the sodium system in performance. The transition frequencies and required power levels are also within the range

1 M. Valet, M. Pinard, and G. Grynberg, *Opt. Commun.* 81: 403 (1991).

2 G. Alzetta, A. Gozzini, L. Moi, and G. Orriols, *Nuovo Cimento B* 36: 5 (1976); H.R. Gray, R.M. Whitley, and C.R. Stroud, *Opt. Lett.* 3: 218 (1978).

3 P.R. Hemmer, D.P. Katz, J. Donoghue, M. Cronin-Golomb, M.S. Shahriar, and P. Kumar, *Opt. Lett.* 20: 982 (1995); T.T. Grove, M.S. Shahriar, P.R. Hemmer, Prem Kumar, V.K. Sudarshanam, and M. Conin-Golomb, *Opt. Lett.* 22: 769 (1997).

4 V.K. Sudarshanam, M. Cronin-Golomb, P.R. Hemmer, and M.S. Shahriar, *Opt. Lett.* 22: 1141 (1997).

5 T.T. Grove, E. Rousseau, Xiao-Wei Xia, D.S. Hsuing, M.S. Shahriar, and P.R. Hemmer, *Opt. Lett.* 22: 1677 (1997).

of diode lasers, potentially allowing inexpensive and practical systems in the future. While this scheme was much simpler than the one employed in sodium, it was still necessary to introduce a detuning (typically 80 MHz) between the two pump beams, in order to provide the symmetry-breaking necessary for this process. Aside from the experimental inconvenience, this nondegeneracy renders this conjugator unsuitable for applications such as phase conjugate resonators.

In this work, we demonstrate how this conjugator can be produced with degenerate frequencies by writing the gratings in a band of atoms moving with non-zero velocities without greatly compromising performance. To illustrate the mechanisms at work in this OPC consider first the role of atomic velocities. Figure 1 shows a j = 1 to j' = 1 atom (with no magnetic field) moving with respect to the laser beams. The Doppler shift seen by each atom is

$$\Delta_F = -kv_z \cos\alpha + kv_x \sin\alpha$$

$$\Delta_S = -kv_z \cos\alpha - kv_x \sin\alpha$$

$$\Delta_F - \Delta_S = 2kv_x \sin\alpha.$$

If $|\Delta_F - \Delta_S|$ is small enough, we satisfy the Raman resonance condition (between F and S) and coherently trap the atom in a super-position of the ground state's Zeeman sublevels (CPT). Since the degenerate Zeeman sublevels correspond to different orientations of angular momentum, it can be shown that there is a sinusoidally varying angular momentum grating formed by F and S.[6] The spacing of this grating is inversely proportional to sin α. The backward pump beam, B, diffracts off the grating and forms the conjugate beam, C. If α is increased, the Doppler shifts from F and S become different for an increasing number of atomic velocity groups; hence, an increasing number of atomic velocity groups are no longer Raman resonant. As such, only a band of atoms within a range of velocities centered around $v_x = 0$ contributes to the conjugation process.

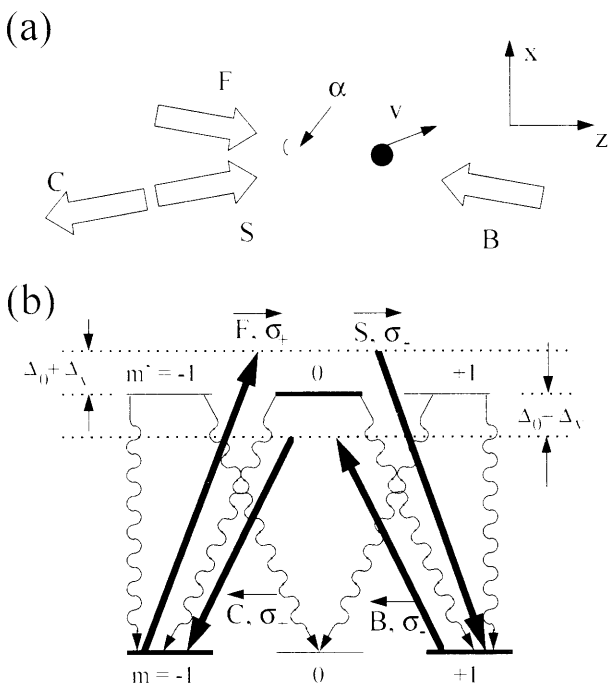

Figure 1. (a) The orientation of the beams involved in the four-wave mixing process; F: forward pump, B: backward pump, S: signal, C: conjugate. (b) The magnetic sublevels involved in the interaction. Here, Δ_O is the laser detuning, and Δ_V is the Doppler shift for an atom moving with velocity v in the z-direction. The fields are all degenerate in the laboratory frame.

All values of v_z satisfy the Raman resonance condition. However, the laser intensity needed for producing the dark state coherence grows quadratically with v_z. For the low laser intensity used, only a band of atoms with a small range of $|v_z|$ contributes to the grating formation. The width of this band is directly proportional to the power-broadening-limited linewidth of the Raman resonance, which is typically about 2 MHz. For the experiment reported in Grove et al.,[7] this band is centered around $v_z = 0$. Thus, the frequency difference between the forward (F) and backward (B) pumps in the frame of the atoms is the same as in the laboratory frame. In the experiment reported here, we make F and B degenerate. Now the Doppler shift from a $v_z \neq 0$ group of atoms provides the effective frequency difference between F and B. However, using a nonzero velocity group reduces the density of atoms which are active in the conjugation process compared to the nondegenerate

6 T.T. Grove, E. Rousseau, Xiao-Wei Xia, D.S. Hsuing, M.S. Shahriar, and P.R. Hemmer, *Opt. Lett.* 22: 1677 (1997).

7 Ibid.

experiment. Thus, the degenerative frequency case reported is not expected to have the same efficiency as the optical conjugator reported in Grove et al.[8] We point out that coherences between Zeeman sublevels were used in many experiments[9] but not for the process reported here.

The experimental setup is shown in Figure 2. A Ti:Sapphire laser and beamsplitters provide all of the input beams: F, B and S. Polarizing beamsplitting cubes are used to combine the beams, and quarter-wave plates are used to create the proper polarizations. The angle between S and F is about 5 mrad. The rubidium cell is a heat pipe oven at a temperature of 142°C with a μ-metal shielded Helmholtz coil to provide a magnetic field.

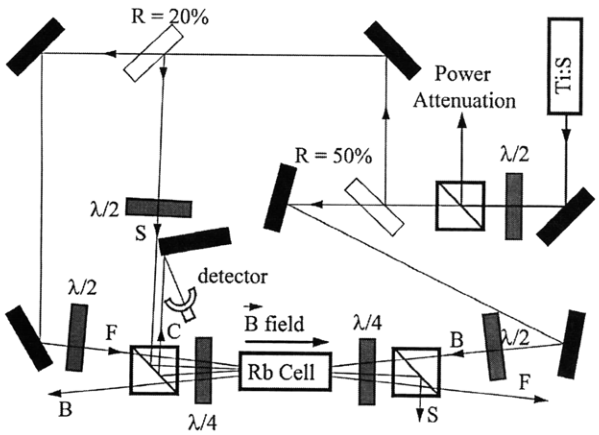

Figure 2. Schematic illustration of the experimental setup. The rubidium cell is a heat-pipe oven, and the pump is a Ti:Sapphire laser. λ/2 is a half-wave plate, and λ/4 is a quarter-wave plate.

Figure 3 shows the reflectivity of the conjugate, as a function of the laser frequency. Here, the first dotted line corresponds to the $5^2S_{1/2}$ F = 2 to $5^2P_{1/2}$ F = 1 transition, and the second dotted line corresponds to the $5^2S_{1/2}$ F = 2 to $5^2P_{1/2}$ F = 2 transition of the D_1 manifold, in ^{87}Rb. Consider first the envelope of the conjugate reflectivity, denoted by the dashed lines. The peak of this curve corresponds to a blue detuning above the F = 2 to F = 1 transition. Consider the three dips in the reflectivity curve. The first and third dips correspond to the situations when the laser frequency is exactly on resonance with the F = 2 to F = 1 transition and the F = 2 to F = 1 transition, respectively. The second dip corresponds to the laser frequency being exactly halfway between these two transitions. For all three of these conditions, the symmetry-breaking is minimized, for atoms at all velocities. The reduction in conjugate reflectivity at these three locations is therefore consistent with our proposed model.

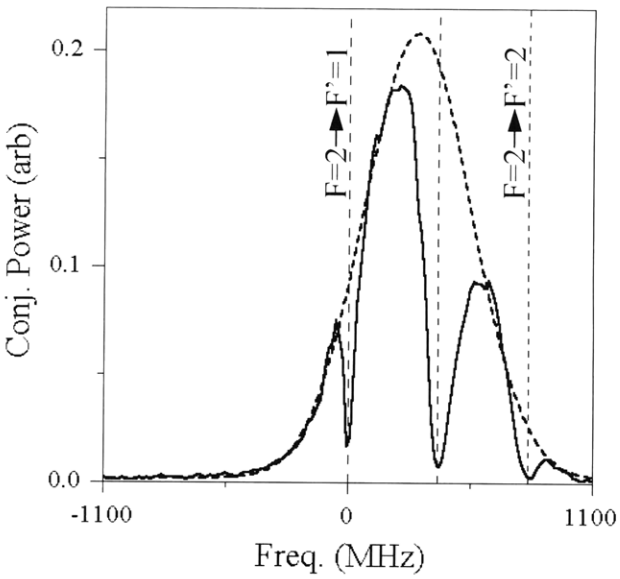

Figure 3. The conjugate power as a function of the laser frequency. The vertical dotted line on the left (right) corresponds to the $5^2S_{1/2}$ F = 2 to $5^2P_{1/2}$ F = 1 ($5^2S_{1/2}$ F = 2 to $5^2P_{1/2}$ F = 2) transition of the D_1 manifold in ^{87}Rb.

Figure 4 demonstrates the dependence of the conjugate reflectivity on the input signal power. As demonstrated in previous work,[10] the conjugate is mainly in the σ_+ polarization component, which is approximately 400 times stronger than the σ_- component. F has a power of 84 mW, and B has a power of 24 mW. The pump intensity imbalance again is consistent with the idea that the conjugation favors asymmetry. The laser frequency is kept on the largest peak shown in Figure 3. We observe a reflectivity as high as 40, saturating to lower values as the probe strength is increased.

8 T.T. Grove, E. Rousseau, Xiao-Wei Xia, D.S. Hsuing, M.S. Shahriar, and P.R. Hemmer, *Opt. Lett.* 22: 1677 (1997).

9 D. Suter, H. Kepel, and J. Mlynek, *Phys. Rev. Lett.* 67: 2001 (1991); F. Renzoni, W. Maichen, L. Windholtz, and E. Arimondo, *Phys. Rev. A* 55: 3710 (1997).

10 Ibid.

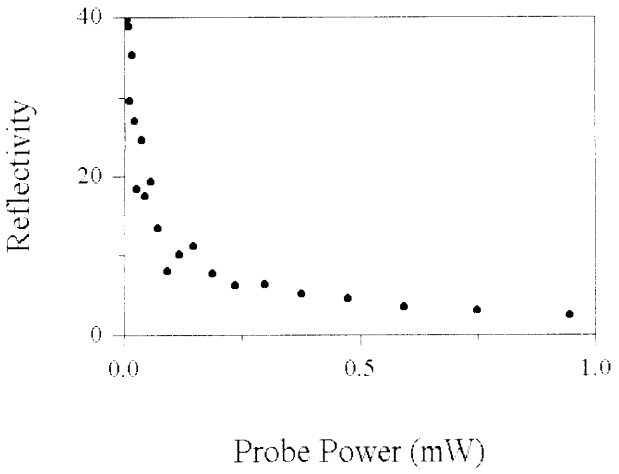

Figure 4. The conjugate reflectivity as a function of the probe power, showing saturation as the probe becomes stronger.

The results in Figure 5 show magnetic field response of the conjugate. For small magnetic fields this is equivalent to detuning the frequency between F and S via the Zeeman shift; hence this is a measurement of the Raman transition width. The FWHM is approximately 1 MHz compared to 2.4 MHz in the nondegenerate case.[11] Both of these results are well below the natural linewidth of 5.9 MHz. If we assume that the optical pumping rate has the dominant effect on the linewidth, we find that the response time is approximately 160 ns.

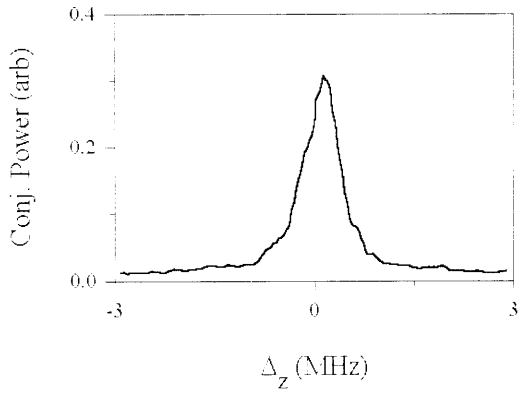

Figure 5. The conjugate reflectivity as a function of two-photon detuning between F and S (Δ_z is the Zeeman shift). The subnatural linewidth of about 1 MHz (FWHM) is consistent with coherent population trapping.

We also examined the dependence of the conjugate on the backward pump polarization (not shown). A $\lambda/2$ plate placed directly before the $\lambda/4$ plate controls the polarization, with the backward beam becoming σ_+ polarized when the $\lambda/2$ plate is rotated 45°. Consistent with predictions, the conjugate beam does not form when the pump beam is incorrectly polarized.

In conclusion, we have observed high reflectivity (>40) optical phase conjugation for a low-pump intensity (10 W/cm^2), using degenerate four-wave mixing in rubidium vapor.

1.1.1 Publications

Grove, T.T., M.S. Shahriar, P.R. Hemmer, Prem Kumar, V.K. Sudarshanam, and M. Conin-Golomb. "Distortion-free Gain and Noise Correlation in Sodium Vapor with Four-wave Mixing and Coherent Population Trapping." *Opt. Lett.* 22: 769 (1997).

Grove, T.T., E. Rousseau, Xiao-Wei Xia, D.S. Hsuing, M.S. Shahriar, and P.R. Hemmer. "Efficient and Fast Optical Phase Conjugation by Use of Two-Photon-induced Grating in the Orientation of Angular Momentum." *Opt. Lett.* 22: 1677 (1997).

Renzoni, F., W. Maichen, L. Windholtz, and E. Arimondo. "Coherent Population Trapping with Losses Observed on the Hanle Effect of the D_1 Sodium Line." *Phys. Rev. A* 55: 3710 (1997).

Sudarshanam, V.K., M. Cronin-Golomb, P.R. Hemmer, and M.S. Shahriar. "Turbulence-aberration Correction with High-Speed High-Gain Optical Phase Conjugation in Sodium Vapor." *Opt. Lett.* 22: 1141 (1997).

1.2 Demonstration of a Phase Conjugate Resonator using Degenerate Four-Wave Mixing via Coherent Population Trapping in Rubidium

Sponsors

U.S. Air Force - Office of Scientific Research/
AASERT
Grant F49620-96-1-0308

U.S. Air Force - Research Laboratory
Grant F30602-97-C-0136

11 D. Suter, H. Kepel, and J. Mlynek, *Phys. Rev. Lett.* 67: 2001 (1991); F. Renzoni, W. Maichen, L. Windholtz, and E. Arimondo, *Phys. Rev. A* 55: 3710 (1997).

1.2.1 Summary

We have demonstrated a ring cavity laser using the gain mechanism of a four-wave mixing process, mediated by two-photon Zeeman coherence resulting from coherent population trapping in a rubidium vapor cell. The cell acts as an amplifying phase conjugate mirror at one corner of the ring cavity. Even though the fundamental process requires nondegeneracy between the probe and the conjugate in the atom's frame, they are degenerate in the laboratory frame, via selection of a moving band of atoms for the gratings. As such, no frequency shifting is necessary in the cavity. The polarization orthogonality of the probe and the conate is compensated by an intra-cavity quarter wave plate.

Details of this work are posted at http://qop.mit.edu/.

1.3 Intracavity High-speed Turbulence Abberation Correction in a Sodium Phase Conjugate Resonator

Sponsor

U.S. Air Force - Rome Laboratory
Grant F30602-97-2-0101
Grant F30602-97-2-0100

Optical cavities bounded by a phase conjugate mirror (PCM) with high gain and a conventional mirror are known[12] to lase even in the presence of intracavity phase aberrations. Such aberration-compensated phase conjugate resonators (PCRs) have also been utilized for other applications such as associative memories,[13] high-resolution optical data processing,[14] and imaging threshold detectors.[15] Among several nonlinear optical materials,[16] the use of sodium vapor as the PCM has been shown[17] to provide gain greater than unity and an ideal response time of about 16 nsec, even with cw pump lasers. Thus, real-time cw aberration correction at high speed and high gain should be possible in a PCR which uses Na vapor as the PCM. Other PCM materials are known[18] to require high-power pulsed lasers for obtaining fast response time and high gain.

A cw PCR using resonant degenerate four-wave mixing (DFWM) in Na vapor was reported. However, this cw PCR laser required very high pump intensities of ~2.5 kW/cm^2 and did not demonstrate the ability to operate with intracavity turbulence.[19] In contrast, we demonstrate in this paper a cw degenerate PCR using Na vapor with a very low lasing threshold of ~4.5 W/cm^2 of pump intensity. Fast spatio-temporal aberration correction is demonstrated in the presence of a high-speed turbulent flow inside the cavity. Such a cw PCR with low-pump intensity is made possible by DFWM based on coherent population trapping (CPT)[20] in Na vapor when operating close to the D_1 transition.

Nondegenerate four-wave mixing (NDFWM)[21] based on CPT involving Raman transitions in Na vapor was shown previously[22] to correct turbulence aberrations in a PCM geometry. A helium jet forced into air at a frequency of 18 kHz and flow velocity of 170 m/s was utilized to demonstrate the spatio-temporal aberration correction. A temporal correction factor of 7.8 was measured at a concurrent power gain of 32 even in the presence of the helium flow. A major difficulty with using such an NDFWM set-up to generate a PCR output at a single frequency is the requirement to match the frequencies of the "probe" and "conjugate" beams. Instead of using an electrooptic modu-

12 See, for example, R.A. Fisher, ed., *Optical Phase Conjugation* (New York: Academic Press, 1983), chapters 13 and 14; R.C. Lind and D.G. Steel, *Opt. Lett.* 6: 554 (1981).

13 A. Yariv and S.-K. Kwong, *Opt. Lett.* 11: 186 (1986).

14 G.J. Dunning, S.W. McCahon, M.B. Klein, and D.M. Pepper, *J. Opt. Soc. Am. B* 11, 339 (1994).

15 M.B. Klein, G.J. Dunning, G.C. Valley, R.C. Lind, and T.R. O'Meara, *Opt. Lett.* 11: 575 (1986).

16 See, for example, R.A. Fisher, ed., *Optical Phase Conjugation* (New York: Academic Press, 1983), chapters 13 and 14.

17 R.C. Lind and D.G. Steel, *Opt. Lett.* 6: 554 (1981); see, for example, B. Monson, G.J. Salamo, A.G. Mott, M.J. Miller, E.J. Sharp, W.W. Clark III, G.L. Wood, and R.R. Neurgaonkar, *Opt. Lett.* 15: 12 (1990).

18 J.R.R. Leite, P. Simoneau, D. Bloch, S. Le Boiteux and M. Ducloy, *Europhys. Lett.* 2: 747 (1986).

19 See, for example, B. Monson, G.J. Salamo, A.G. Mott, M.J. Miller, E.J. Sharp, W.W. Clark III, G.L. Wood, and R.R. Neurgaonkar, *Opt. Lett.* 15: 12 (1990).

20 H.R. Gray, R.M. Whitley, and C.R. Stroud, *Opt. Lett.* 3, 218 (1978); E. Arimondo, in *Progress in Optics XXXV*, E. Wolf, ed. (Elsevier, New York, 1996), pp.258-354.

21 P.R. Hemmer, D.P. Katz, J. Donoghue, M. Cronin-Golomb, M.S. Shahriar and P. Kumar, *Opt. Lett.* 20, 982 (1995).

22 V.S. Sudarshanam, M. Cronin-Golomb, P.R. Hemmer and M.S. Shahriar, *Opt. Lett.* 22, 1141 (1997).

lator in the PCR path to match the two frequencies, we demonstrate here high-gain DFWM based on CPT, which we use to construct a PCR with an intracavity turbulent jet.

In the PCR experimental arrangement shown in Figure 6, the linearly polarized output of a cw dye laser is split by the beam splitter BS1 into the forward F and backward B pump beams counterpropagating in the Na vapor cell. The dye laser is tuned close to the Na D_1 transition. The pumps F and B are slightly focused by lenses L (f = 1 m) to a FWHM diameter of 660 μm at the cell center. An optical isolator I prevents feedback into the dye laser from reflections. A PCR cavity is formed between the high-reflectivity (95%) output coupler R and the Na cell acting as the high-gain PCM. In the presence of an aberrator in the PCR path, the PCR beam A entering the cell would be aberrated, and the PCR beam C leaving the cell would be corrected after passing through the aberrator. The conjugate PCR beam C is generated primarily by the scattering of B from the grating formed by F and A. The frequencies of the PCR beams A and C generated in this DFWM arrangement are the same as that of F and B. The PCR beam is cross-polarized relative to both F and B. The use of the polarizing beam splitters, PBS, facilitates the steering of A into the cell and the separation of C from B. The portion of A transmitted through the cell is denoted by "T" and can exhibit amplification under conditions of gain in the DFWM interaction. The PCR beams A and C are aligned to intercept F and B in the cell at a vertical angle of about 8.5 mrad. The typical FWHM diameters of F and B at the center of the cell are ~0.66 mm, while that of A and C are ~0.23 mm. The typical optical intensity of F and B at the cell center is about 10 W/cm^2 each, unless otherwise stated. The intensity of the PCR beam at the cell center is estimated to be ~2.6 W/cm^2 at the maximum PCR power of 1.7 mW. The Na vapor cell is a heat-pipe oven operated at ~260°C with an ambient pressure of ~18 mTorr. No buffer gas is added to the cell. Stray magnetic fields are reduced to less than 20 mG with the use of magnetic shielding around the cell. A telescope, TL, enables mode-matching within the PCR cavity.

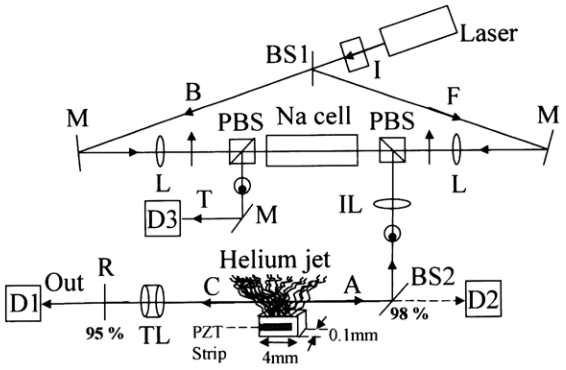

Figure 6. Schematic of the experimental arrangement for a degenerate PCR with intracavity turbulence aberration correction.

A turbulent jet is placed 1m away from a lens IL (f = 25 cm) which images the jet into the cell with a demagnification of ~67%. This jet is obtained by forcing helium gas at room temperature through a rectangular nozzle (4 mm x 0.1 mm). The 4 mm side of the nozzle is aligned along the PCR path. The nozzle is placed ~3 mm below the PCR beam path. The nozzle is driven by a PZT transducer at its resonance frequency of 17.8 kHz. The average helium flow speed at the nozzle exit is estimated from the flow rate of 16 cubic foot per hour and the area of the nozzle (0.5 mm^2) to be ~250 m/s.

A CCD camera is utilized to demonstrate spatial aberration correction. The profile of the compensated PCR beam is sampled by the CCD camera at D1, and the aberrated PCR beam profile is sampled at D2. The CCD camera is placed 1.92 m away from the jet when placed at D1 and 0.57 m away from the jet at D2. Temporal aberration is measured by directing the PCR output at R (or BS2) onto a 0.3 mm pinhole mounted on a photodetector. For the temporal aberration measurements, the PDA replaces the CCD camera at the locations D1 and D2. The transverse location of the PDA is adjusted for maximum amplitude at 17.8 kHz. The ratio of this peak-to-peak ac voltage to the maximum voltage level is termed the modulation depth. This is chosen as the experimental measure of the temporal aberration at the forcing frequency because it compensates for any difference in the intensities of C and A.

Spatial aberration correction is demonstrated in Figure 7 through time-averaged CCD images. The beam profiles are shown both as two-dimensional contour plots at intervals of 20% of the peak intensity, and as one-dimensional line traces of the intensity at the highest peak location in each profile. The profile of the PCR beam A sampled at D2 is shown in Figure 7a with the helium flow ON and OFF, while that of the compensated PCR beam C sampled at D1 is shown in Figure 7b under the same flow conditions. As seen from Figure 7b, a well-corrected nearly-circular spot is seen at the output coupler R on double-pass through the jet, whereas the uncompensated PCR beam A is severely aberrated by the helium jet. The difference in the sizes of the beams C and A shown in Figure 7a is due to the convergence of A as it approaches the imaging lens, IL, from the telescope, TL, and the different distances of D1 and D2 on opposite sides of the jet. The profile of the transmitted PCR beam, T, is sampled at the location D3 which is 0.54 cm away from the cell center (Figure 6 and is shown in Figure 7c with the flow ON and OFF. As expected, the transmitted PCR beam, T, is aberrated by the flow in like manner to A. In the presence of the helium flow, the power in the PCR beams C and A was reduced to half the power with the flow turned off.

Fast temporal aberration correction at 17.8 kHz is demonstrated in Figure 8 through plots of the instantaneous output voltage from the PDA. Here, Figure 8a shows the effect of turbulence on the aberrated PCR beam A, while Figure 8b shows that for the compensated PCR beam, C. From this data, the signal modulation depth in A is estimated at ~63.6%, whereas that in C is ~6.6%, demonstrating that temporal aberrations are corrected by a factor of ~9.6 in the PCR output at R. As discussed in G. Grynberg et al.,[23] resonances at higher vibration frequencies result in subharmonics at the output of the PDA and thus are not useful for the measurement of the modulation depth.

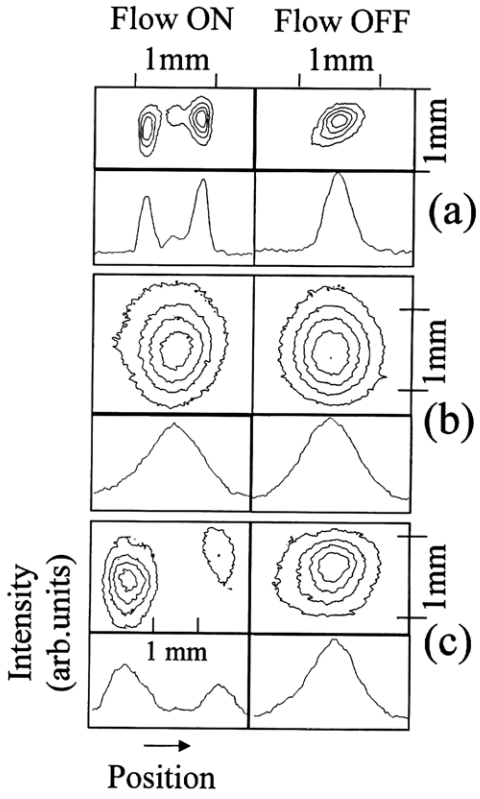

Figure 7. Data showing spatial aberration correction: 2D contours (upper plots) and 1D line traces (lower plots) of the intensity profile of (a) the aberrated PCR beam A, (b) the compensated PCR beam C, and (c) the transmitted PCR beam T. Contour lines are drawn at 80, 60, 40 and 20% of peak intensity.

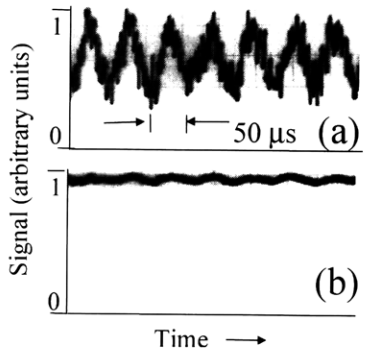

Figure 8. Temporal aberration correction: PPD signal showing turbulence effects on (a) aberrated PCR beam A and (b) the compensated PCR beam C.

23 G. Grynberg, E. Le Bihan, P. Verkerk, P. Simoneau, J.R.R. Leite, D. Bloch, S. Le Boiteux, and M. Ducloy, *Opt. Commun.* 67: 363 (1988).

In contrast to the NDFWM configuration in G. Grynberg et al.,[24] degenerate pumps are used in this DFWM set-up. In order to establish that the system is indeed based on purely DFWM and not NDFWM, the optical frequencies of the PCR beams C and A are determined by mixing with a probe beam, P (not shown in Figure 6). For this purpose, a small portion of F is tapped off and shifted in frequency by 5 MHz. Such a small shift in optical frequency is achieved by passing the probe beam successively through two acousto-optic modulators (AOMs) driven at 294 and 299 MHz. Figure 9 shows the frequency spectrum recorded at the output of an avalanche photodiode (APD) on which the two beams C and P are mixed. Figure 9b shows the electrical spectrum of a beat detector mixing the drive frequencies applied as input to the two AOMs. Similar spectra are obtained when A is mixed with P. The 5 MHz separation of the peaks in Figure 9a and Figure 9b establishes that DFWM indeed gives rise to C and A. It is also seen from Figure 9a that the PCR output spectrum shows only a single peak. Thus, the PCR is oscillating in a single longitudinal mode even without the use of frequency-selective elements within the lasing cavity. For the cavity length of 2.1 m used here, the expected[25] PCR longitudinal mode spacing (c/4L) is ~36 MHz. Multiple longitudinal modes are not supported in our PCR because the two-photon bandwidth of the CPT interaction is far lesser, as discussed later.

Figure 10a shows the optical power in the PCR beam C as a function of the pump laser frequency. The peaks named I, J, and K can be selectively enhanced in power at their respective frequencies by changing the alignment angle between C (A) and the pumps F and B. Aberration correction measurements described in this paper are done with the peak I enhanced as it occurs at the largest angle of ~8.5 mrad from the pumps, thus keeping away from the angular range of conical emission[26] that occurs when the pumps are tuned close to the peak K. This conical emission has a typical half-angle of ~5 mrad or less.

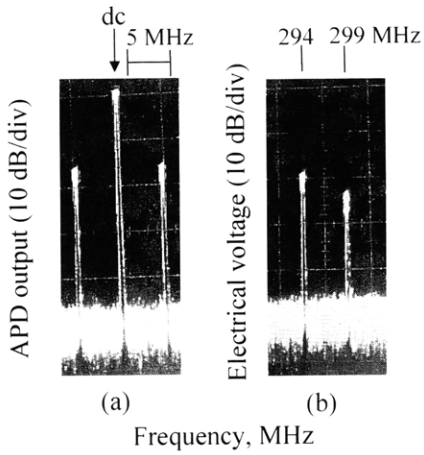

Figure 9. Verification of DFWM: (a) the optical beat between C (or A) and the probe P (shifted by 5 MHz from F), and (b) the electrical voltage spectrum of the two AOM drive signals at 294 and 299 MHz used to generate P.

When the peak K is enhanced, the angular location of the PCR beams is seen to nearly coincide with the lobes in the hexagonal pattern characteristic of such conical emission. The small broadened peaks between J and K are from diffuse conical emission that is primarily orthogonal in polarization to the PCR beams. The peak I is enhanced when the pump laser frequency is red-detuned by ~300 MHz from the F = 2 to the F' = 1 transition. It should be noted that the Doppler width of Na vapor at 260°C is ~1.1 GHz. Therefore, the detuning measured applies only to the zero-velocity group in the vapor.

24 G. Grynberg, E. Le Bihan, P. Verkerk, P. Simoneau, J.R.R. Leite, D. Bloch, S. Le Boiteux, and M. Ducloy, *Opt. Commun.* 67: 363 (1988).

25 R.C. Lind and D.G. Steel, *Opt. Lett.* 6: 554 (1981).

26 D. Suter, H. Kepel, and J. Mlynek, *Phys. Rev. Lett.* 67: 2001 (1991); F. Renzoni, W. Maichen, L. Windholtz, and E. Arimondo, *Phys. Rev. A* 55: 3710 (1997); see, for example, R.A. Fisher, ed., *Optical Phase Conjugation* (New York: Academic Press, 1983), chapters 13 and 14.

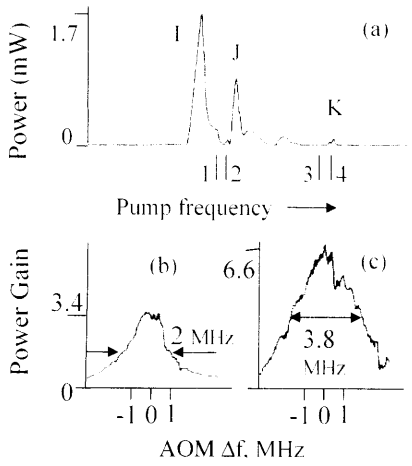

Figure 10. (a) PCR intracavity power as a function of the pump frequency. The numbers 1 through 4 correspond to the following D_1 transitions: (1) F = 2 $\leftrightarrow$ F′ = 1 (2) F = 2 $\leftrightarrow$ F′ = 2 (3) F = 1 $\leftrightarrow$ F′ = 1, and (4) F = 1 $\leftrightarrow$ F′ = 2. (b) The PCM conjugate gain as a function of Δf for the two pump intensities (1) 4.6 W/cm^2 and (2) 10 W/cm^2.

The threshold pump intensity at which the PCR output becomes unstable in time was determined (with the flow OFF) by attenuating the total pump power obtained from the laser. The laser frequency was kept fixed at the peak I shown in Figure 5a. The threshold intensity for each pump was found to be 4.5 W/cm^2.

To test for CPT, a probe beam, P, with variable frequency relative to F was conjugated. The output coupler R was misaligned to stop oscillation in the PCR mode. However, the experimental operating conditions for this "PCM" mode remained similar to that for the PCR. The conjugate power gain showed peaks at the same frequencies as I, J, and K shown in Figure 10a. The laser was tuned to the frequency for peak I. As described earlier, the frequency of P was varied by using the set of two AOMs. Figure 10b and Figure 10c show the conjugate power gain as a function of the difference frequency between F and P, for two different powers of F. In Figure 10b a maximum gain of 3.4 for a probe power of 90 μW is seen at zero difference frequency. The FWHM of the gain is ~2 MHz, far less than the 10 MHz excited state decay rate of Na. This subnatural radio-frequency linewidth for the two-photon interaction is taken as direct evidence for Raman CPT. Another test[9] for Raman CPT is the dependence of the FWHM on the generalized Rabi frequency. As shown in Figure 10b and Figure 10c, the power-broadened linewidth of 2 MHz increases to 3.8 MHz when the pump intensity increases from 4.6 W/cm^2 to 10 W/cm^2. In order to test the double-Λ nature of the CPT-based DFWM interaction,[11] the conjugate and the probe beams are mixed on an APD. When P is shifted by 1 MHz from F (and B), C is found shifted by 2 MHz from the probe and by 1 MHz from F (and B).

In conclusion, a low-threshold PCR based on DFWM involving a double-Λ CPT interaction has been presented, in which temporal aberrations caused by intracavity turbulence at a frequency of 18 kHz and high speed of 250 m/s have been corrected by a factor of 9.6.

1.4 Frequency-selective Time-domain Optical Data Storage by Electromagnetically Induced Transparency in a Rare-earth Doped Solid

Sponsors

National Science Foundation
Grant ECS 94-21304
U.S. Air Force - Office of Scientific Research
Grant F49620-96-1-0395
U.S. Air Force - Rome Laboratory
Grant F30602-96-2-0100

Since the proposal[27] and subsequent experimental demonstration of stimulated photon echoes in both vapors[28] and solids,[29] there has been increasing interest in their use for high-capacity optical data storage. Much of this interest arises from the large theoretical storage density available in rare-earth doped solids, given by the ratio of optical inhomogeneous to homogeneous widths, which can be in excess of 10^{30}. However, for rare-earth doped solids, this storage density is generally only available at

27 T.W. Mossberg, *Opt. Lett.* 7: 77 (1982).

28 N.W. Carlson, L.J. Rothberg, A.G. Yodh, W.R. Babbitt, and T.W. Mossberg, *Opt. Lett.* 8: 483 (1983).

29 M.K. Kim and R. Kachru, *Opt. Lett.* 12: 593 (1987).

30 G. Alzetta, A. Gozzini, L. Moi, and G. Orriols, *Nuovo Cimento B* 36: 5 (1976); H.R. Gray, R.M. Whitley, and C.R. Stroud, Jr., *Opt. Lett.* 3: 218 (1978).

temperatures below 4 K and decreases rapidly at higher temperatures due to the increase of homogeneous width by phonon interactions. In addition, some of the most widely used rare-earth doped solids require highly frequency-stable lasers to approach theoretical storage densities.[31] To overcome these limitations, we proposed[32] a technique to store optical data using spin coherences excited by coherent population trapping,[33] which in the present context is equivalent to electromagnetically induced transparency (EIT).[34] The advantages are that spin coherences tend to have much longer lifetimes than optical coherences at higher temperatures and that EIT can be made to be insensitive to laser jitter.

In this report, we experimentally demonstrate frequency-selective time-domain optical data storage in Pr^{3+}:Y_2SiO_5 (Pr:YSO) using spin echoes excited by EIT. We verify the key prediction that the theoretical storage density does not significantly degrade with increasing crystal temperature up to 6 K. In contrast, at this temperature, the theoretical optical storage density determined by the photon echoes is more than an order of magnitude smaller than its value below 4 K (as will be discussed later). We also verify the predicted insensitivity of theoretical storage density to laser frequency jitter.

The optical storage technique described in this report is analogous to the frequency-selective stimulated photon echo memory.[35] With this technique, the optical inhomogeneous width is chopped into M accessible channels in the frequency domain, and each channel is used for N-bit data storage in the time domain. Ideally, the Fourier component of each data pulse (and any laser frequency jitter) should be narrower than the assigned channel width. It is easy to show that the maximum storage density, NM, is given by the ratio of optical inhomogeneous to homogeneous widths. The length of the time domain "write window" is given by the optical transverse relaxation time T_2. In the present experiment, the time-domain portion of the memory utilizes a ground-state spin coherence rather than an optical one. This means that the time domain "write window" is now given by the spin T_2, which is generally longer than optical T_2, especially at higher temperatures or if there is appreciable laser jitter. Furthermore, if the inhomogeneous width of the spin transition is equal to or wider than the assigned optical frequency channel, then the theoretical storage density of the new technique is given by the ratio of the optical inhomogeneous width to the spin homogeneous width. This is nearly always larger than the theoretical optical photon echo storage density, especially at high temperatures.

For the detection of frequency-selective stimulated spin echoes excited by EIT, we use enhanced nondegenerate four-wave mixing (NDFWM).[36] The advantage of this technique is to increase echo detection efficiency as shown in a previous paper.[37]

Figure 11 shows energy level diagram of 0.05 at. % Pr doped YSO in which the optical transition frequency of $^3H_4 \rightarrow {}^1D_2$ is 605.7 nm. The splittings of the ground-hyperfine states are 10.2 MHz and 17.3 MHz as shown.[38] The time-dependent coherence σ_{12} between the ground states $|1\rangle \leftrightarrow |2\rangle$ in Figure 11 is created by the two resonant optical fields ω_1 and ω_2 according to the following density matrix equation:

$$d\sigma_{12}/dt = -iD_{13}E_1\sigma_{32}(t)/\hbar + iD_{23}E_2\sigma_{13}(t)/\hbar - \lambda_{12}\sigma_{12}(t)$$

where D_{ij} is dipole matrix element corresponding to the transition $|i\rangle \rightarrow |j\rangle$, and γ_{12} is the decay rate of σ_{12}. E_1 and E_2 are (slowly varying) pulse amplitudes of the electric fields of the laser beams at ω_1 and ω_2, respectively. Since the ground state coherence term σ_{12} is directly coupled to the optical coherences σ_{13}

31 X.A. Shen, E. Chiang, and R. Kachru, *Opt. Lett.* 19: 1246 (1994).

32 P.R. Hemmer, M.S. Shahriar, B.S. Ham, M.K. Kim, Y. Rozhdestvensky, *Mol. Cryst. Liq. Cryst.* 291: 287 (1996).

33 G. Alzetta, A. Gozzini, L. Moi, and G. Orriols, *Nuovo Cimento B* 36, 5 (1976); H.R. Gray, R.M. Whitley, and C.R. Stroud, Jr., *Opt. Lett.* 3: 218 (1978).

34 K.-J. Boller, A. Imamoglu, and S.E. Harris, *Phys. Rev. Lett.* 66: 2593 (1991); B.S. Ham, P.R. Hemmer, and M.S. Shahriar, *Opt. Comm.*, forthcoming; S.E. Harris, J.E. Field, and A. Imamoglu, *Phys. Rev. Lett.* 64: 1107 (1990); B.S. Ham, M.S. Shahriar, and P.R. Hemmer, *Opt. Lett.* 22: 1138 (1997).

35 T.W. Mossberg, *Opt. Lett.* 7: 77 (1982).

36 S.E. Harris, J.E. Field, and A. Imamoglu, *Phys. Rev. Lett.* 64: 1107 (1990); B.S. Ham, M.S. Shahriar, and P.R. Hemmer, *Opt. Lett.* 22: 1138 (1997).

37 B.S. Ham, M.S. Shahriar, M.K. Kim, and P.R. Hemmier, Opt. Lett. 22:1849 (1997).

38 K. Holliday, M. Croci, E. Vauthey, and U.P. Wild, *Phys. Rev. B.* 47: 14741 (1993).

and σ_{23}, time dependent phenomena can be predicted using perturbation theory as in two level systems.[39]

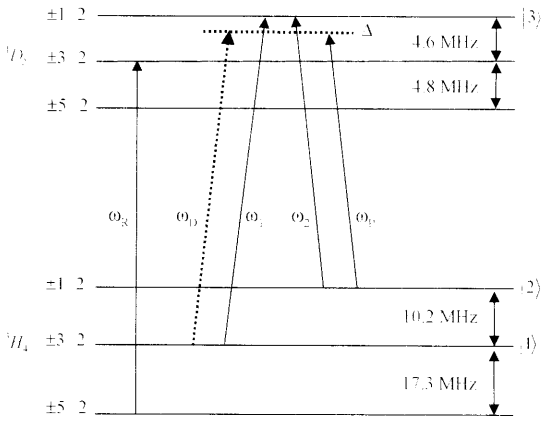

Figure 11. Energy level diagram of Pr:YSO.

To probe the ground state coherence, a probe beam ω_P is red-detuned by Δ = 1.5 MHz from the frequency of the beam ω_2, as shown. A repump beam ω_R is used to provide frequency selectivity in the inhomogeneously broadened optical transition as discussed elsewhere.[40] The repump beam is chosen to excite a different transition than the two beams ω_1 and ω_2 to escape from coherent interactions. A stimulated spin echo (rephased coherence σ_{12}) is produced by three resonant raman pulses each having two frequencies ω_1 and ω_2 and is detected by NDFWM using ω_P to generate the signal beam ω_D which is proportional to the rephased spin coherence.

Figure 12 shows a schematic of the experimental setup. A frequency stabilized cw ring dye laser is pumped by an argon-ion laser. The dye laser has jitter of ~1 MHz which is measured using a Febry-Perot spectrum analyzer. We use acousto-optic modulators (AOM) driven by frequency synthesizers to make four coherent laser beams ω_1, ω_2, ω_R, and ω_P from the dye laser output as shown. The laser powers of the beams ω_R, ω_1, ω_2, and ω_P are ~10, 30, 2, and 10 mW, respectively. The use of AOMs makes laser jitter correlated so that laser difference frequencies are stable typically down to sub-kHz. The angle between the beams ω_1 and ω_2 is ~60 mrad. The direction of the probe beam is chosen to satisfy Bragg matching, but is not exactly co-propagating with either beams ω_1 or ω_2 (see inset in Figure 12). The diffracted beam ω_D, which is generated from NDFWM process, satisfies the phase matching condition of $\vec{k}_D = \vec{k}_1 + \vec{k}_2 - \vec{k}_P$. All laser beams are forward propagating, circularly polarized with a quarter wave plate, and focused into the sample (Pr:YSO) by a 40 cm focal length lens. The measured beam diameters (1/e in intensity) of the beams are ~150 μm in the crystal. The size of the crystal is 3×6×9 mm with its symmetric optical B-axis along the 9 mm direction, and it is mounted inside a cryostat. To pulse the laser beams, rf switches driven by pulse generators (SRS DG 535 and HP 214 A) are used. The repetition rate of these pulses is 100 Hz. To average the laser jitter noise, thirty diffracted signals are detected by a fast silicon photo-diode (Thorlabs PDA 150) and averaged by a Boxcar averager (SRS 250) with a gate width of 3 μs.

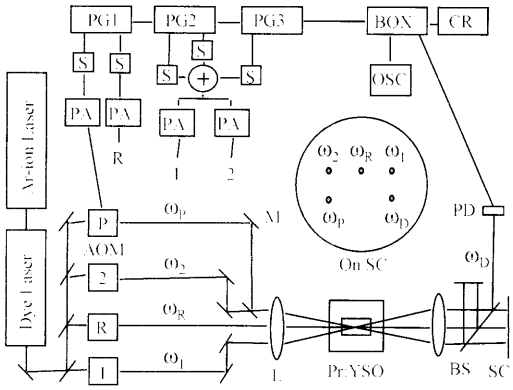

Figure 12. Schematic of the experimental setup for frequency-selective time-domain stimulated spin echo by EIT; AOM, acousto-optic modulator; BOX, boxcar averager; BS, beam splitter; CR, chart recorder; L, lens; M, mirror; OSC, oscilloscope; PA, rf power amplifier; PD, photo diode; PG, pulse generator; S, rf switch; SC, screen.

Figure 13 shows the storage of two bits of time-domain optical data by frequency-selective stimulated spin echoes based on EIT. For this data, the crystal temperature is 6 K. Each input pulse is composed of both resonant Raman beams ω_1 and ω_2. The first two input pulses (d and d') are data bits. The second and third input pulses are write (w) and read (r) pulses, respectively. The pulse width of the

39 M. Mitsunaga and R.G. Brewer, *Phys. Rev. A* 32: 1605 (1985).

40 B.S. Ham, M.S. Shahriar, M.K. Kim, and P.R. Hemmier, Opt. Lett. 22:1849 (1997).

repump beam is 1 ms (not shown) and immediately precedes the data pulse d. The pulse widths of the data bits (d and d') are 7 μs and 2 μs, respectively, separated by 100 μs. The widths of the write and read pulses (w and r) are 7 μs and 5 μs, respectively, separated by 1.1 ms which is twice the spin T_2. The time delay between data pulse d' and the write pulse w is 300 μs, which is chosen to be longer than the optical T_2 (111 μs) but shorter than the spin T_2. The probe pulse width is 5 μs, and the diffracted signals (30 samples) are averaged by the Boxcar averager. When the input pulses are present, the diffracted signals are off-scale on the chart recorder. As seen in Figure 13, there are "two-pulse" echoes just after the write pulse w. The echo signal e is bigger than e' because the data d has a wider area than d'. The stimulated echoes are retrieved by the read pulse r at $t_3 + t_2$ and $t_3 + t_2 - t_1$. Their intensities are comparable with those of the "two-pulse" echoes. The theoretical storage time is limited by a spin population decay time T_1, which is ~100 s in this material[41] but is several hours in Eu:YSO.[42] The storage density of the spin transition is determined by the ratio of spin T_2 to T_2*. This ratio can be made large by applying a magnetic field to slow down the spin T_2,[43] or by using a magnetic field gradient to create additional inhomogeneous broadening.[44]

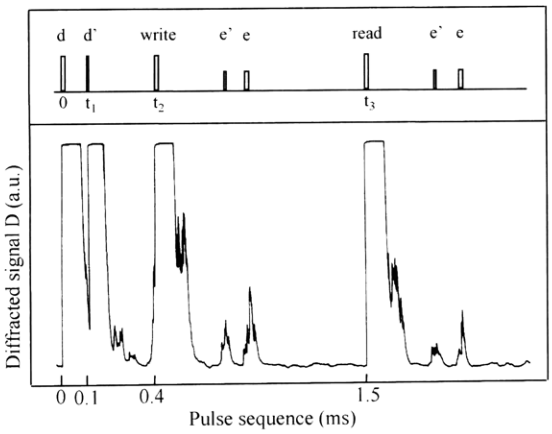

Figure 13. Two-bit optical data storage by frequency-selective time-domain stimulated spin echo based on EIT at 6 K: d and d', data; e and e', echoes.

Figure 14a shows the spin T_2 versus temperature. Each spin T_2 is measured from the "two-pulse" echo intensity (see e in Figure 13) versus the write pulse delay t_2 with pulses d' and r absent. We varied the write pulse delay time from 100 μs to 900 μs. Fluctuations in Figure 14 are caused by laser jitter which affects the observed echo signal intensity. Within the measurement fluctuations, the spin T_2 appears constant up to 6 K.

To infer how the optical T_2 depends on temperature, we simply measure the intensity of "two-pulse" echo at a fixed write pulse delay t_2 (Figure 14b). The pulse delay t_2 is kept at 400 μs. The echo intensity should be proportional to the square of the optical T_2, since the efficiency of EIT depends on the product of Ω^2 and the optical T_2, where Ω is the rms Rabi frequency for the transitions at ω_1 and ω_2.[45] As we see in Figure 14b, the echo intensity decreases exponentially above 4 K. This implies that the optical T_2 also decreases exponentially as temperature goes up. Beyond 6 K, the signal was too weak to measure the spin T_2 with our low-sensitive photodiode, even though we detected the echoes until the spectral hole-burning phenomenon persisted (~8 K).

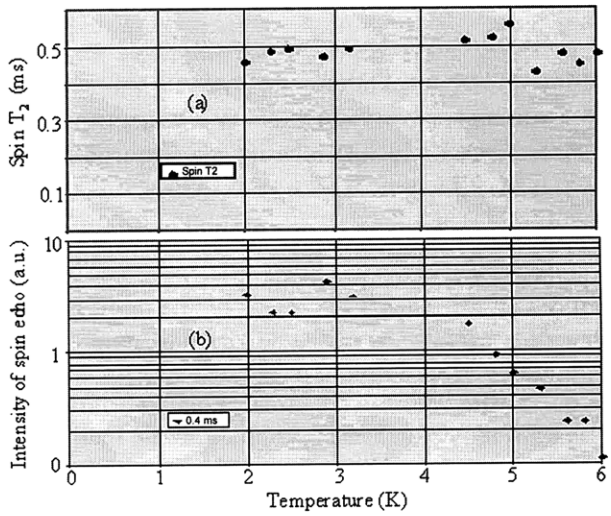

Figure 14. (a) Spin T_2 versus temperature. (b) Inferred optical T_2 versus temperature.

41 K. Holliday, M. Croci, E. Vauthey, and U.P. Wild, *Phys. Rev. B.* 47: 14741 (1993).

42 R. Yano, M. Nitsunaga, and N. Uesugi, *Opt. Lett.* 16: 1884 (1991).

43 R.M. Macfarlane, C.S. Yannoni, and R.M. Shelby, *Opt. Comm.* 32: 101 (1980).

44 P.R. Hemmer, K.Z. Cheng, J. Kierstead, M.S. Shahriar, and M.K. Kim, *Opt. Lett.* 19: 296 (1994).

45 P.R. Hemmer, M.S. Shahriar, V.D. Natoli, and S. Ezekiel, *J. Opt. Soc. Am.* B 6: 1519 (1989).

In summary, we observed frequency-selective time-domain optical data storage using EIT excited spin echoes in Pr:YSO at 6 K. The echoes are detected using NDFWM enhanced by EIT. We showed that the write window is determined by the spin T_2 which is much longer than the optical T_2 especially at higher temperature. We also measured the spin T_2 and found it almost constant in the range of 2-6 K. In contrast, at temperatures above 4 K, we observed that the optical T_2 decreases exponentially as temperature goes up. Therefore these results demonstrate the potential of higher capacity optical data storage than by conventional photon echo methods in rare-earth doped solids at high temperatures.

1.4.1 Publications

Ham, B.S., M.S. Shahriar, and P.R. Hemmer. "Enhanced Nondegenerate Four-Wave Mixing Owing to Electromagnetically Induced Transparency in a Spectral Hole-burning Crystal." *Opt. Lett.* 22: 1138 (1997).

Ham, B.S., P.R. Hemmer, and M.S. Shahriar. *Opt. Comm.* 144: 227 (1997).

1.5 Spin Coherence Excitation and Rephasing with Optically Shelved Atoms

Sponsors

National Science Foundation
Grant ECS 94-21304
U.S. Air Force - Office of Scientific Research
Grant F49620-96-1-0395
U.S. Air Force - Rome Laboratory
Grant F30602-96-2-0100

1.5.1 Summary

We have investigated the use of resonant optical Raman pulses to excite and rephase ground state spin coherence via the partial storage or shelving of atoms. Unlike rf excited spin echoes or off-resonant Raman echoes, the resonant Raman optical field does not directly excite the spin coherence. Rather, an optical π-pulse shelves part of the atoms in an excited state, leaving behind a net spin coherence. Efficient rephasing can be accomplished with a Raman resonant optical 2π-pulse due to 180 degree phase shift incurred after one Rabi flop. In a crystal of Pr^{3+}-doped Y_2SiO_5, we experimentally observe spin echo efficiency as high as 46% of the free induction decay signal.

Details of this work are posted at http://qop.mit.edu/.

1.6 Long-Term Optical Data Storage in Thick Holograms

Sponsor

U.S. Air Force - Office of Scientific Research/
AASERT
U.S. Ballistic Missile Defense Organization

The five-dimensional data storage scheme discussed above would be useful as a dynamic memory, using optical pulses. On the other hand, many applications require long-term data storage. The ability to store a large number of holograms in a single recording material is important for the implementation of optical neural networks, optical interconnects, and holographic computing elements. Recently, a strong effort[46] has been undertaken by several groups to develop high-volume data storage devices using holograms. The fundamental storage capacity in such a system is limited to $\sim V/\lambda^3$, where V is the volume, and λ is the wavelength of light. In practice, this limit is difficult to achieve, due primarily to cross-talks. Various techniques, including angle multiplexing, wavelength multiplexing, orthogonal phase encoding, and fractal-space multiplexing, or a combination thereof have been employed to improve the storage density, although still well below the theoretical limit.

For practical systems of wider use, it is necessary to develop holographic storage systems that will work at room temperature. In principle, a thickness of between 1 and 2 cm provides optimum storage density, due to constraints imposed by optical access requirements. Data storage using holograms of such thickness (1 cm or more) have so far only been performed in photorefractive crystals. However, photopolymeric systems generally have several distinct advantages over photorefractive systems. These include much lower cost, lack of constraint in shape, higher diffraction efficiency, lower refractive index

46 F.H. Mok, *Opt. Lett.* 18: 915 (1993); S. Tao, D.R. Selviah, and J.E. Midwinter. *Opt. Lett.* 18: 912 (1993); A. Chiou, *Opt. Lett.* 17: 1018 (1992); G. Rakuljic, V. Leyva, and A. Yariv. *Opt. Lett.* 17: 1471 (1992); H. Li and D. Psaltis. *Appl. Opt.* 33: 3764 (1994); H. Yu, S. Li, and D. Psaltis, *J. Opt. Soc. Am. A* 12: 1902 (1995).

(1.6, compared to 2.2 for typical photorefractives) which implies a larger field of view, simplicity of fixing, and a wide spectral bandwidth (400 to 1500 nm). As such, these materials can be used to make a practical disc memory, read by compact semi-conductor lasers. For example, the lasers currently used in CD ROMS operate near 800 nm, which is near the peak of the photopolymer sensitivity, but is outside the spectral response curve of Lithium Niobate crystals.

However, to date, only thin (100 μm or less) holograms have been successfully used to demonstrate storage in photopolymeric structures.[47] This is due to a host of problems in creating thick holograms of good quality. These problems span issues such as differential shrinkage, non-uniformity of active elements through the substrate, difficulty in embedding materials into substrates, and lack of high quality optical surfaces. As a result, the full potential of holographic data storage in such media is kept limited by the useful thickness. For example, the storage achievable in a 100 μm-thick hologram is theoretically two orders of magnitude smaller than what can be achieved in a 1 cm-thick hologram. Even within the current limits due to optical accessing architectures, it should be possible to store as much as 150 bits/μm^2 in a 1 cm-thick hologram.

In recent years, many groups around the world have been trying to develop thick photopolymeric holograms suitable for data storage. Arguably, one of the leaders in this pursuit has been the Vavilov State Optical Institute. Very recently, they have succeeded in developing novel thick holographic material called photopolymer with diffusion amplification (PDA).[48] This material has an excellent surface quality, causes very low scattering, and has a diffraction efficiency nearing 100%, with negligible loss.

This material consists of phenanthraquinone embedded in polymethylmethacrylate (PMMA). This medium uses the novel principle of diffusion amplification of holograms on polymeric recording media. Briefly, photoexposure of this system results in writing of two out-of-phase periodic structures that partially compensate each other. One of these is formed by a concentration distribution of chromatophore groups combined into macromolecules, while the other is formed by free molecules. As a result of diffusion of the free molecules, the corresponding grating degrades, and the resulting grating is amplified without additional processing. The surviving grating is stored in macromolecules that do not diffuse.

We have recently developed specialized methods for creating samples of this material suitable for optical memory. A typical hologram of PDA is a cylidrical disc with a diameter of 10 cm and a thickness of 5 mm (compared to 100 μm for photopolymeric discs currently used). With peristropic and angular multiplexing, such a system will have a net storage capacity of more than 10^{12} bits (>100 Gbytes), estimated conservatively within the currently accepted limits due to optical accessing limitations. We use a Argon laser to write the holograms. The holograms are cured *in situ* with ease, and without causing any degradation. The read-out system may use single-mode semiconductor lasers at 800 nm, along with other electronic and optical components such as SLMs and CCD cameras.

Previously, we have written holograms in a sample 1.5 mm-thick, in order to determine the number of holograms that can be superimposed using angular multiplexing.[49] Very recently, we have written a set of ten high resolution images using angle multiplexing. Figure 15 shows one of the typical original and reconstructed images, with no noticeable distortions. Figure 16 shows the efficiency of the ten holograms as a function of readout angle (5 mrad between each hologram), illustrating virtually zero cross-talk. This result bodes well for our initial goal of achieving a raw bit error rate (BER) of 10^{-5}, so that with error-correction-codes the real bit error rate can be made as low as 10^{-12}. Once this is achieved, we will work on demonstrating an operational memory disk with a capacity of at least 100 Gbytes and an access rate of 1 Gbit/sec.

47 A. Pu and D. Psaltis, in *Proceedings of OSA* Annual Meeting, Portland, Oregon, 1995 (MEE4); B. Kohler, S. Bernet, A. Renu, and U. Wild, *Opt. Lett.* 18: 2144 (1993).

48 A.V. Veniaminov, V.F. Goncharov, and A.P. Popov, *Opt. Spectroscopy* (USSR) 70(4): 505-08 (1991), and references therein.

49 10. J.E. Ludman, J.R. Riccobono, H.J. Caulfield, J.M. Fournier, I.V. Semenova, N.O., Reinhand, P.R. Hemmer, and S.M. Shahriar, in *Proceedings of IS&T Conference*, San Jose, California, February 1995; H. Kogelnik, *Bell Syst. Tech. J.* 48: 2909 (1969).

(a)

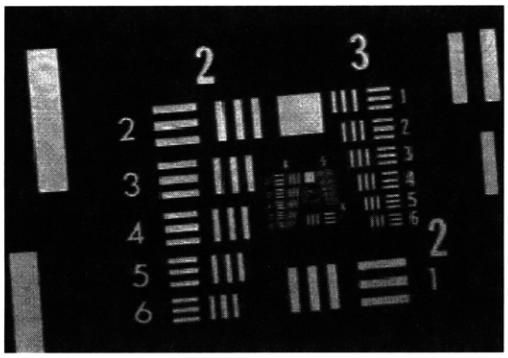

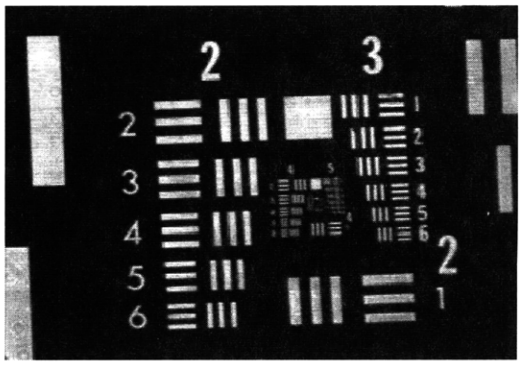

(b)

Figure 15. High-fidelity reproduction of a sample of the ten-angle multiplexed optical images stored in a thick PDA substrate.

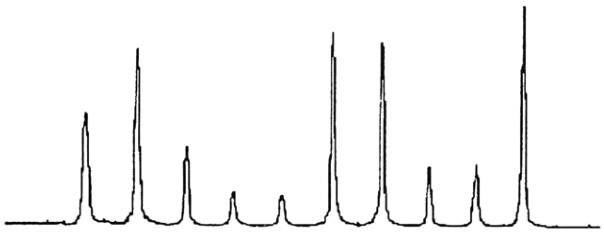

Figure 16. Efficiency of the ten holograms as a function of readout angle (5 mrad between each hologram), illustrating virtually zero cross-talk.

1.7 Atomic Interferometry for Nanolithography and Nonlinear Atom Optics

Sponsors

U.S. Air Force - Office of Scientific Research
Grant F49620-95-1-0510

U.S. Army Research Office

1.7.1 Summary

Previously, we reported experimental results of an experiment where blazed gratings produced by optical standing waves are used to split an atomic beam of metastable helium. Given the limits of the optical power available from the LNA laser, we were able to demonstrate a splitting of $\pm 20\ \hbar k$, where $\hbar k$ is the linear momentum of a photon. In principle, however, this process is capable of producing splittings as large as $\pm 200\ \hbar k$.

Currently, we are working on using this scheme to create this kind of beam splitter using rubidium atoms. The high power available from a Ti:Sapphire laser makes it possible to achieve the large amount of splitting mentioned above. Once the split atoms are recombined, they interfere to produce fringes. For the $\pm 200\ \hbar k$ splitting, the fringe spacing is less than 2 nm. By using multiple zones of beam splitting, it becomes possible to get fringes that are less than a nm wide.

A key requirement for this project is a high flux supersonic beam. We have finished construction of such a beam, which employs three separate zones, each evacuated by a separate diffusion pump. Argon gas at twice the atmospheric pressure is used to seed the flow. In the zone following the supersonic expansion, we maintain a pressure of 10^{-4} Torr. The pressure beyond the second skimmer is 10^{-6} Torr, and the interaction zone has a pressure of 10^{-8} Torr. During the preliminary run, we have seen a high flux beam up to the first collimating slit. Work is underway to improve the alignment of the second collimation slit with respect to the first one.

We are also developing a source of rubidium Bose condensate atoms, in order to perform nonlinear mixing of atomic beams, using a (two-photon) laser beam as the mixing mediator. To this end, we have (1) achieved magneto-optic trapping from a vapor background, (2) slowed a rubidium beam using chirped cooling, and (3) constructed an Ioffe-Pritchard type magneto optic trap with very strong fields. These three segments have now been combined, and the whole system has been pumped down to 1×10^{-11} Torr, a vacuum level necessary for achieving Bose condensation.

Details on this work are posted at http://qop.mit.edu/.

1.8 Multi-atom Quantum Bits and Cavity Dark States for Quantum Computing in Spectral Holeburning Media

Sponsor

U.S. Air Force - Office of Scientific Research
Grant F49620-96-1-0395

1.8.1 Summary

We have developed a scheme for creating a nontrivial number of qubits (quantum bits) using dark resonance techniques, in which two optical fields are used to turn a quantum system transparent by creating a coherent superposition of internal states. Specifically, we explore the following schemes.

In one approach, we use a dark resonance where the quantum system consists of two groups of spectrally separated atoms inside an inhomogeneously broadened medium, such as a Pr:YSO spectral hole burning (SHB) crystal, and the photon number state in a single mode of a cavity. Adiabatic transitions are used to transfer quantum information between the two groups of atoms, as well as to realize quantum logic gates. Unlike models presented previously by Pellizzari et al., here the classical field applied externally has two distinct frequency components, which overlap each other spatially. Furthermore, each qubit is represented collectively by a group of atoms numbering N, prepared by optical pumping to be in a pure state, and the atoms couple the cavity state containing zero photons to that containing N photons. Since the number of atoms in each spectral hole is generally more than one, such an approach is necessary for realizing qubits in an SHB medium. We will use a cryogenically cooled, thin layer of Pr:YSO, embedded in a cavity, to implement this scheme. We have recently demonstrated near perfect dark resonances in this system. For the parameters of this medium, the number of coupled qubits that can be prepared this way is about 400.

In another approach, we will use a dark resonance technique where the quantum system consists of two spatially separated atoms and the photon number state in a single mode of a cavity. By detuning the classical fields while keeping the cavity resonant, we have found theoretically that we can produce a dark state which contains no photons in the cavity mode (a cavity dark state). The advantage of this scheme is that the quantum decoherence time is not limited by the cavity decay time. This idea can also be extended to the case of coupling two spectrally adjacent groups of atoms.

Details on this work are posted at http://qop.mit.edu/.

1.9 Fiberoptic Damage Detection

Sponsor

Idaho National Energy Laboratory

Project Staff

Niell G. Elvin

Structural and mechanical failure of construction materials is typically characterized by the gradual fatigue growth of cracks and damaged zones within the material. The early detection through monitoring of subsurface damage (such as delamination) can prevent final failure of structural components. Although a myriad of nondestructive techniques are available for monitoring structural integrity, these techniques are generally expensive and are unsuitable for monitoring large structural components. Fiberoptic sensors can potentially offer a solution to existing structural integrity monitoring problems due to their high sensitivity, low weight, immunity to electromagnetic interference such as lightning, continuous monitoring capabilities, their ability to detect distributed strains over large distances and their cheap price. This ongoing research effort focuses on theoretical electromechanical analysis and experimental verification to provide guidelines for the design and placement of fiberoptic sensors.

In previous work,[50] theoretical analysis and experimental verification of a novel moving load method has been described which allows for the detection of the extent and position of damage. The location and size of damage can be garnered by the monitoring of the integrated strain while moving a load over the damaged site. Figure 17 shows a schematic repre-

50 N. Elvin, C. Leung, V.S. Sudarshanam, and S. Ezekiel, "A Novel Fiber Optic Delamination Detection Technique. Part 2: an Experimental Feasibility Study," submitted to *J. Intel. Mat. Syst. Struct.*; N. Elvin and C. Leung, "A Novel Fiber Optic Delamination Detection Technique. Part 1: a Theoretical Feasibility Study," submitted to *J. Intel. Mat. Syst. Struct.*; N. Elvin and C. Leung, "Feasibility Study of Delamination Detection with Embedded Optical Fibers." *J. Intel. Mat. Syst. Struct.*, forthcoming.

sentation of a Mach-Zender interferometer with active servohomodyne demodulation which can be used to determine the strain differences of damaged and undamaged structural component.

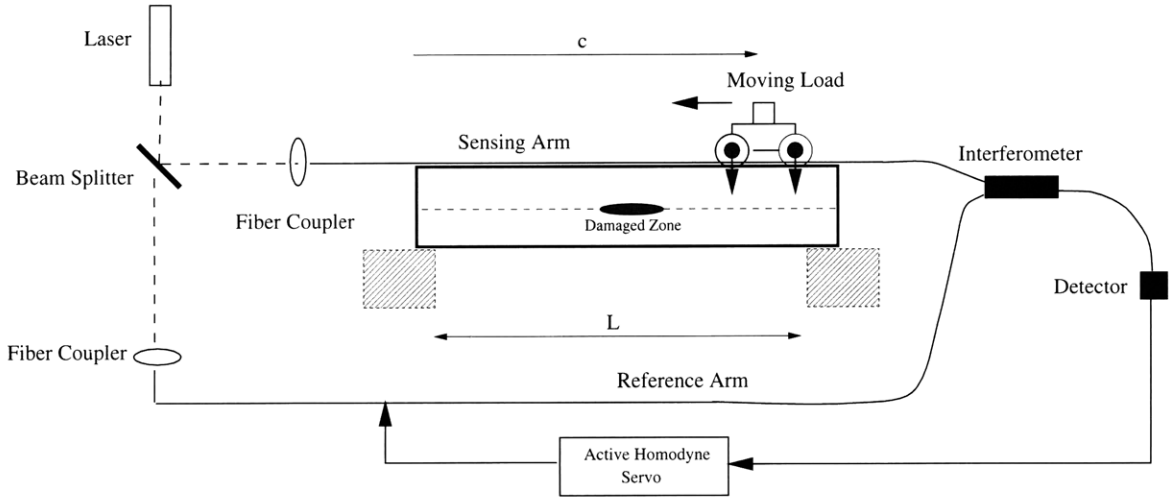

Figure 17. Schematic representation of interferometer used for damage detection.

Our previous work has focused on detection of relatively large voids in structural components. The ongoing work is to detect and characterize small scale defects in which nonlinear mechanical behavior can be expected. Figure 18 shows a typical application of small scale damage detection in which a rolling load can cause fretting fatigue of its riding surface.

Final material failure can occur in the form of spalling when cracks grow and reach the surface. This problem is nonlinear since the crack faces are in contact and subjected to friction. The feasibility of detecting such small scale, nonlinear defects is our ongoing research initiative.

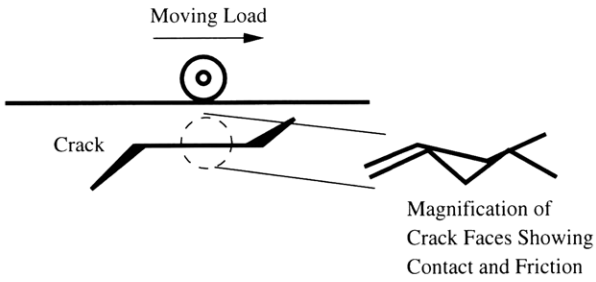

Figure 18. Rolling fretting fatigue causing nonlinear mechanical behavior through contact and friction.

1.9.1 Publications

Elvin, N., and C. Leung. "A Novel Fiber Optic Delamination Detection Technique. Part 1: a Theoretical Feasibility Study." Submitted to *J. Intel. Mat. Syst. Struct.*

Elvin, N., C. Leung, V.S. Sudarshanam, and S. Ezekiel. "A Novel Fiber Optic Delamination Detection Technique. Part 2: an Experimental Feasibility Study." Submitted to *J. Intel. Mat. Syst. Struct.*

Elvin, N., and C. Leung. "Feasibility Study of Delamination Detection with Embedded Optical Fibers." *J. Intel. Mat. Syst. Struct.* Forthcoming.